Effect of internal resistance of a Helmholtz resonator on acoustic energy reduction in enclosures

Ganghua Yu, Deyu Li, and Li Cheng[a)]
Department of Mechanical Engineering, The Hong Kong Polytechnic University, Hung Hom, Kowloon, Hong Kong, SAR of China

(Received 1 April 2008; revised 21 August 2008; accepted 4 September 2008)

The effect of internal resistance of a Helmholtz resonator on acoustic energy reduction in an enclosure and the multimodal coupling-based Helmholtz resonator design are investigated. Using the analytical solution of a resonator-enclosure interaction model, an energy reduction index is defined in a frequency band to optimize the resonator resistance. The dual process of energy dissipation and radiation of the resonator is quantified. Optimal resistance of the resonator and its physical effect on the resonator-enclosure interaction are numerically evaluated and categorized in terms of frequency bandwidths. Predictions on the resonator performance are confirmed by experiments. Comparisons with existing models based on different optimization criteria are also performed. It is shown that the proposed model serves as an effective design tool to determine the internal resistance of the resonator in order to achieve sound reduction in the frequency band enclosing acoustic resonances. © *2008 Acoustical Society of America.* [DOI: 10.1121/1.2996328]

PACS number(s): 43.50.Gf, 43.50.Jh, 43.20.Ks [KA] Pages: 3534–3543

I. INTRODUCTION

Studies on Helmholtz resonators (HRs) have been arousing persistent interest for many decades as evidenced by a large body of existing literature. On one hand, HRs have been extensively used to control noise transmissions in various systems such as ducts, cylindrical shells,[1] ducts,[2] and double panels.[3] On the other hand, they have also been used as sound amplifying devices to perform energy conversion of different types as shown by some very recent work.[4–6] Irrespective of applications, the design of HRs with suitable characteristics has always been a key issue. Effort has been made not only on the development of prediction models[7,8] but also on the design and realization of HRs.[9]

Early work concerning HR coupled to an enclosure can be traced back to Van Leeuwen who proposed a design chart based on electrical circuit analogy.[10] Due to the simplicity of the HR, its use was found in controlling the interior noise inside an enclosure. It was also observed, however, that the proposed design chart in Ref. 10 might lead to an apparent discrepancy with experiments at enclosure resonances.[11] Subsequently, Fahy and Schofield proposed another model to improve the work in Ref. 10 by taking into account the coupling between a single resonator and a single enclosure mode of interest.[11] By maximizing the energy dissipation of the resonator at the targeted frequency, a formula was proposed to determine the Q-factor of the resonator. They cautioned, however, that the resonator designed using their formula might not lead to the maximum reduction in sound pressure level (SPL) inside the enclosure around the targeted frequency. To cover the small frequency range around the targeted frequency, which can be loosely called "broad band," they equalized the dominant peaks inside the band and provided an equation to determine the Q-factor of the resonator. Also in that work, three different types of damping materials were used in the resonator to improve the dissipation and to broaden the working bandwidth. Experimental results showed that the performance of the resonator was reduced by either excessive or insufficient damping of the resonator. Proper damping materials were experimentally determined to achieve an optimal reduction in SPL around the targeted resonance inside the enclosure. Recently, similar observations were made by Slaton and Zeegers in their experimental work on a flow-duct system with a damped HR.[12] The existence of an optimal value of the resonator resistance has been clearly shown in their experiments. Fahy and Schofield's work is important in that it provides insightful information to guide the resonator design. It also sets an important milestone in the HR design that, even nowadays, is still being used.[1,13] Meanwhile, their work also shows the need for a general model to count for the acoustic interaction among resonators and multiple acoustic modes of the enclosure. With a view to further increase the control performance, Cummings[14] extended Fahy and Schofield's model to multiple resonators, along with the consideration of multiple modes of the enclosure. By considering resonators as pseudo pulsating sphere sources, characterized by the averaged sound pressure over the surface of the sphere, the singularity problem in the equation set was avoided. However, this treatment of the equivalent sphere induced a large discrepancy between the predicted coupled frequencies and the measured ones.[15] Recently, a new model was proposed by Li and Cheng[15] to analyze the interaction between an acoustic resonator array and an enclosure with multiple modes. Different from Ref. 14, they solved the interaction equation inside the enclosure to obtain the modal responses and employed these modal responses to find the sound pressures at the resonator apertures. This avoided the singularity problem encountered in Ref. 14 when calculating the sound pressure at the center of a point source radiated by its own. Comparisons between

a)Electronic mail: mmlcheng@polyu.edu.hk

theoretical and experimental results showed that the model provides a good approximation to real multimode setup.

Despite the persistent effort made in the past, researchers still need ways and tools to achieve optimal design of HRs, which right now still involves extensive experimental measurements on a trial-and-error basis. It is known that resonators interact with the enclosure through dissipating energy on one hand and radiating energy back to the enclosure on the other hand. A clear demarcation and quantification of these two effects may be one of the key elements to explain the way in which an optimally designed resonator works. On the other hand, insertions of acoustic resonators create new peaks around the original targeted peak, which are referred to as coupled or newly emerged peaks hereafter.[11,13] An ideal resonator design should target a frequency band including both targeted and coupled resonance peaks. Upon enlarging the frequency band of interest, the possible multimodal coupling effect on the resonator design needs to be qualified and somehow be taken into account in the design process. Unfortunately, these issues have not been fully investigated even up to now, mainly due to the lack of reliable, yet simple enough model.

The model proposed by Li and Cheng[15] admits analytical solutions when only one HR is involved, such providing an opportunity for the aforementioned issues to be addressed. This paper attempts to explore this unique feature of the model and makes contributions in the following aspects: (1) a systematic demarcation and quantification of the energy radiation and dissipation effect of the resonator when coupled to a multimodal enclosure; (2) determination of the internal resistance of the resonator to ensure the maximum sound energy reduction (ER) inside the enclosure within a frequency band around a targeted resonance frequency, along with experimental validations; (3) qualification of the impact of the frequency band and the modal coupling on resonator design; and (4) reassessment of the existing models through comparisons with the present one. These analyses are believed to shed light on the underlying physics of the HRs coupled to an acoustic enclosure and bring significant improvement on the existing knowledge on HR design for acoustic ER in enclosures.

II. THEORY

The system under investigation comprises a rigid-walled acoustic enclosure with a classical HR. The resonator consists of a cavity of volume V^R with a neck of area S^R and effective length L^R, as shown in Fig. 1. Throughout the paper, the superscripts and subscripts E, R, and S indicate variables associated with "enclosure," "resonator," and "source," respectively. In this section, an ER index is established based on the analytical solutions. Formulas for calculating dissipation energy and radiation energy from an HR are derived, which depend on the internal resistance of the resonator.

A. Energy radiation and dissipation of HR

When installing a resonator in an enclosure having a primary sound source, the vibration of the lumped mass in the resonator neck radiates sound back to the enclosure, resulting in an acoustic interaction with the enclosure. Meanwhile, energy dissipation also takes place inside the resonator neck. This dual process occurs simultaneously and depends on the property of the resonator, particularly the particle velocity strength in the resonator neck and the internal resistance of the resonator. The lumped mass inside the resonator neck follows Newton's second law and the sound pressure inside the enclosure is governed by the wave equation. Assuming that all time dependent variables are harmonic, after expending the sound pressure p inside the enclosure over a basis of enclosure eigenfunctions $\varphi_j(\mathbf{r})$ as $p=\sum_{j=1}^{J}P_j\varphi_j(\mathbf{r})$ (J is the maximum number of the truncated mode series) and applying orthogonality properties, analytical solutions of the volume velocity source strength $\tilde{Q}^R$ directed outward of the resonator into the enclosure and the jth modal pressure response P_j of the enclosure are, respectively, obtained as[15]

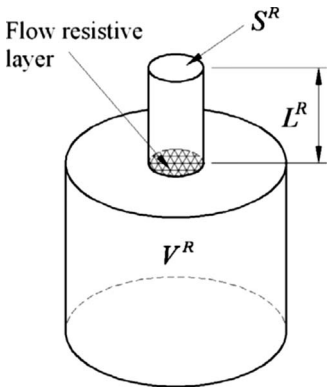

FIG. 1. A damped classical Helmholtz resonator.

$$\tilde{Q}^R=\frac{A^R\frac{V^R}{V^E}\sum_{h=1}^{J}\left[\frac{\omega^2}{\omega^2-(\gamma_h^E)^2}\frac{\varphi_h(\mathbf{r}^R)}{\Lambda_h}\tilde{\varphi}_h(\mathbf{r}^S)\tilde{Q}^S\right]}{1-A^R\frac{V^R}{V^E}\sum_{h=1}^{J}\left[\frac{\omega^2}{\omega^2-(\gamma_h^E)^2}\frac{\varphi_h^2(\mathbf{r}^R)}{\Lambda_h}\right]}, \tag{1}$$

$$P_j=\underbrace{-\frac{i\omega\rho_0}{k^2V^E}\frac{\omega^2}{\omega^2-(\gamma_i^E)^2}\frac{\tilde{\varphi}_j(\mathbf{r}^S)}{\Lambda_j}\tilde{Q}^S}_{\text{contribution from primary source}}$$

$$\underbrace{-\frac{i\omega\rho_0}{k^2V^E}\frac{\omega^2}{\omega^2-(\gamma_j^E)^2}\frac{\varphi_j(\mathbf{r}^R)}{\Lambda_j}\tilde{Q}^R}_{\text{contribution from resonator}}, \tag{2}$$

where

$$A^R=\frac{(\omega^R)^2}{\omega^2-icR\omega-(\omega^R)^2},$$

$\tilde{Q}^S$ is the volume velocity source strength of the primary source located at $\mathbf{r}^S$; $\mathbf{r}^R$ is the location of the resonator; V^E is the volume of the enclosure; γ_j^E is the jth eigenvalue of the enclosure expressed as $\gamma_j^E=\omega_j^E+iC_j^E$, in which the real part is the angular frequency and the imaginary part is an equivalent

ad hoc damping coefficient; $\Lambda_j=\int_{V^E}[\varphi_j(\mathbf{r})]^2 dV/V^E$; $\tilde{\varphi}_j(\mathbf{r}^S)$ is the averaged $\varphi_j(\mathbf{r}^S)$ over the volume of the primary source;[14] z_0 is the characteristic impedance of the air $(\rho_0 c)$; $R=R_i/z_0 L^R$, with R_i being the specific acoustic resistance of the resonator; and $\omega^R=c(S^R/L^R V^R)^{1/2}$, which is the uncoupled resonance frequency of the HR.

Equation (2) provides an analytical solution in terms of modal pressure response inside the enclosure under the effect of the resonator. It also provides insightful information about the interaction between the resonator and the enclosure. The first term on the right hand side of Eq. (2) represents the effect of the primary sound source and the second term characterizes the effect of inserting an acoustic resonator. As expected, the resonator is coupled with all acoustic modes of the enclosure. If a targeted enclosure mode is well separated from other enclosure modes, the interaction among these modes and the resonator can be neglected.[11] On the contrary, high modal density or a larger frequency band of interest may necessitate the consideration of the interaction among the resonator and multiple modes of the enclosure. Same applies if the control performance of the resonator should be evaluated in a broad band. Equation (2) also shows that, when the resonator location is fixed, the internal resistance of the resonator, through A^R, plays an important role in determining the effect of the resonator. An excessively high internal resistance renders A^R approach to zero, such annulling the effect of the resonator. On the contrary, if the internal resistance is too low, A^R tends toward infinity at the resonance frequency, which causes unacceptable high amplitude P_j at the two newly emerged frequencies (coupled peaks) after the resonator is installed.[13] None of the two above scenarios is desirable. Therefore, the internal resistance of the resonator needs to be investigated and properly chosen.

1. Energy radiation from resonator aperture

The sound energy radiated from the resonator is determined by shutting down the primary source in the enclosure. In this circumstance, only the vibration of the mass inside the resonator neck acts as the sound source, which has been previously determined under the presence of the primary source. Setting $\tilde{Q}^S$ to zero in Eq. (2), the modal response P_j^R caused by the resonator radiation alone is calculated as

$$P_j^R=\frac{\omega^2}{\omega^2-(\gamma_j^E)^2}A^R\frac{V^R}{V^E}\frac{\varphi_j(\mathbf{r}^R)}{\Lambda_j}\sum_{h=1}^{J}\varphi_h(\mathbf{r}^R)P_h, \tag{3}$$

where P_h is computed from Eq. (2) when keeping $\tilde{Q}^S$, which is used to calculate the initial displacement and velocity of the lumped mass inside the resonator neck. The acoustic pressure purely created by the resonator radiation is expressed as

$$\hat{p}(\mathbf{r})=\sum_{j=1}^{J}P_j^R\varphi_j(\mathbf{r}). \tag{4}$$

In a typical sound field, the fluctuation of the entropy is usually small compared with that of the pressure. Therefore, the influence of entropy deviation can be neglected, and the energy radiated from the resonator in a period T can be calculated as[16]

$$E_{\text{radi}}^R=w+w_d, \tag{5a}$$

where w is the time-averaged acoustic energy inside the enclosure, including kinetic and potential energy, and w_d is the time-averaged energy dissipation inside the enclosure, which can be determined using the measured Q-factor of the enclosure Q^E as[16]

$$w_d=\frac{\pi S^E}{4Q^E}\frac{w}{V^E}, \tag{5b}$$

where S^E is the surface area of the enclosure. Alternatively, w_d can also be evaluated by adding the energy loss at the boundaries of the enclosure and inside the enclosure caused by thermal conduction and viscosity:

$$w_d=\int_0^T\int_{S^E}\left[\underbrace{\left(\frac{\omega\rho_0\mu}{8}\right)^{1/2}\hat{\mathbf{v}}_T(\mathbf{r}^S)\cdot\hat{\mathbf{v}}_T^*(\mathbf{r}^S)+(\gamma-1)\left(\frac{\omega\rho_0\kappa}{8c_p}\right)^{1/2}}_{\text{Energy loss at boundaries}}\frac{|\hat{p}(\mathbf{r}^S)|^2}{(\rho_0 c)^2}\right]dSdt$$
$$+\int_0^T\int_{V^E}\left[\underbrace{\frac{\kappa}{T_0}(\nabla T')^2}_{\text{thermal conduction loss}}+\underbrace{\mu_B(\nabla\cdot\mathbf{v})^2+\frac{1}{2}\mu\sum_{ij}\alpha_{ij}^2}_{\text{viscosity loss}}\right]dVdt, \tag{5c}$$

where μ is the shear viscosity, $\mathbf{v}$ is the particle velocity, $\hat{\mathbf{v}}_T$ is the tangential component of the amplitude of velocity $\mathbf{v}$ on the enclosure boundary, γ is the specific heat ratio, κ is the coefficient of thermal conductivity, c_p is the specific heat coefficient at constant pressure, T_0 is the ambient temperature, T' is the temperature perturbation given by $p\sqrt{T_0(\gamma-1)/c_p/\rho_0 c}$, μ_B is the bulk viscosity, and α_{ij} is the rate of shear tensor, which is computed from the particle velocity $\mathbf{v}$ as[16]

$$\alpha_{ij}=\frac{\partial v_i}{\partial x_j}+\frac{\partial v_j}{\partial x_i}-\frac{2}{3}\nabla\cdot\mathbf{v}\delta_{ij}\quad(i,j=1,2,3),$$

where x_i apply to x, y, and z and v_i to the component of $\mathbf{v}$ in x, y, and z directions when i equals to 1, 2, 3, respectively.

The time-averaged acoustic energy w over a volume V is calculated by

$$w=\int_V\frac{1}{4\rho_0 c^2}\left[\left(\frac{c}{\omega}\right)^2\nabla\hat{p}\cdot\nabla\hat{p}^*+|\hat{p}|^2\right]dV. \tag{6}$$

The first item in Eq. (6) is the time-averaged kinetic energy and the second item is the time-averaged potential energy. When the volume is the volume of the whole enclosure V^E, Eq. (6) yields

$$w=\frac{V^E}{4\rho_0 c^2}\left[\frac{1}{\omega^2}\sum_{j=1}^{J}(\omega_j^E)^2(P_j^R)^2\Lambda_j+\sum_{j=1}^{J}(P_j^R)^2\Lambda_j\right]. \tag{7}$$

2. Energy dissipation by resonator

The energy dissipated by the resonator in a period T is computed by

$$E_d^R = -\frac{1}{2}\int_0^T \int_{S^R} \mathrm{Re}[p(\mathbf{r}^R)v^*(\mathbf{r}^R)]dSdt, \tag{8}$$

where v is the amplitude of particle speed.

Substituting $p(\mathbf{r}^R)=ZS^R v(\mathbf{r}^R)$ into Eq. (8) yields

$$E_d^R = -\frac{1}{2}S^R \int_{S^R} T|v(\mathbf{r}^R)|^2 \mathrm{Re}(Z)dS, \tag{9}$$

where Z is the acoustic impedance of the HR (Ref. 14)

$$Z = -\frac{R_i}{S^R} - i\left(\frac{L^R\rho_0\omega}{S^R} - \frac{\rho_0 c^2}{V^R\omega}\right). \tag{10}$$

Under the lumped mass assumption, the dissipated energy is calculated from

$$E_d^R = \tfrac{1}{2}S^R R_i T|v(\mathbf{r}^R)|^2, \tag{11}$$

where $|v(\mathbf{r}^R)|^2$ is computed as

$$|v(\mathbf{r}^R)|^2 = \frac{1}{(\rho_0 L^R)^2}\frac{\omega^2|\Sigma_{h=1}^J \varphi_h(\mathbf{r}^R)P_h|^2}{[(\omega^R)^2-\omega^2]^2+(cR\omega)^2}. \tag{12}$$

Substituting Eq. (12) into Eq. (11) and replacing T by $2\pi/\omega$ yield

$$E_d^R = \frac{\pi S^R}{\rho_0 L^R}\frac{cR\omega}{[(\omega^R)^2-\omega^2]^2+(cR\omega)^2}\left|\sum_{h=1}^J \varphi_h(\mathbf{r}^R)P_h\right|^2. \tag{13}$$

If only jth mode of the enclosure is considered, the dissipated power by the resonator at the targeted resonance frequency ($\omega=\omega_j=\omega^R$) is simplified from Eq. (13) as

$$PW_d^R = \frac{E_d^R}{T} = \frac{S^R}{2\rho_0 L^R}\frac{1}{cR}|\varphi_i(\mathbf{r}^R)P_j(\omega^R)|^2. \tag{14}$$

From Eq. (2), the modal response at this natural frequency can be expressed as

$$\frac{P_j}{\tilde{\varphi}_j(\mathbf{r}^S)\tilde{Q}^S} = \frac{cz_0 Q_j^E}{\omega^R V^E \Lambda_j^E}\frac{1}{1+Q^R Q_j^E \varepsilon^2}, \tag{15}$$

where ε^2 is the coupling parameter which equals to $\varphi_j^2(\mathbf{r}^R)V^R/\Lambda_j V^E$, Q^R is the Q-factor of the resonator without its radiation resistance, which is calculated by $Q^R=\omega^R/cR$, and Q_j^E is the Q-factor of the jth enclosure mode given by $Q_j^E=\omega^R/2C_j^E$, in which C_j^E is the jth equivalent *ad hoc* damping coefficient of the enclosure. Without resonator, the modal response of the enclosure at the resonator location is

$$\frac{P_j^0}{\tilde{\varphi}_j(\mathbf{r}^S)\tilde{Q}^S} = \frac{cz_0 Q_j^E}{\omega^R V^E \Lambda_j^E}. \tag{16}$$

Substituting Eqs. (15) and (16) into Eq. (14), the power dissipated by the resonator at the resonance frequency of the jth enclosure mode is determined as

$$PW_d^R = \frac{S^R}{2\rho_0 L^R}\frac{Q^R}{\omega^R}\left|\frac{1}{1+Q^R Q^E \varepsilon^2}\right|^2 |P_j^0\varphi(\mathbf{r}^R)|^2$$
$$= \frac{S^R}{2\rho_0 c k_j L^R}\left|\frac{Q^R}{1+Q^R Q^E \varepsilon^2}\right|^2 |p^{R_0}|^2, \tag{17}$$

where k_j is the wave number at the natural frequency of the jth mode and p^{R_0} is the pressure at the resonator location. When only one targeted mode is considered, the above equation leads to the same expression given in Ref. 11.

B. Quantification of band-averaged performance of HR

In order to achieve a good control performance in the vicinity of the targeted frequency, an "energy reduction index" was defined in a frequency band around the targeted frequency, which was used as the object parameter to optimally determine the internal resistance of the resonator. Upon obtaining the modal response from Eq. (2), the acoustic energy inside the enclosure can be directly computed from Eq. (6). The averaged energy within a frequency band $[\omega_1,\omega_2]$ is defined as

$$E^R = \frac{1}{\omega_2-\omega_1}\int_{\omega_1}^{\omega_2} w d\omega. \tag{18}$$

The frequency band $[\omega_1,\omega_2]$ is chosen to include major frequency components in the vicinity of the targeted original resonance peak (such as the coupled resonance frequencies due to the insertion of the resonator). When computing w using Eq. (6), volume V can either be the local volume or the whole enclosure, depending on whether a local or global sound attenuation is expected. The ER index is defined as

$$\mathrm{ER} = -10\log_{10}\frac{E^R}{E^0}, \tag{19}$$

where E^R and E^0 are energy terms with and without a resonator, respectively.

III. SIMULATIONS AND EXPERIMENTAL VALIDATION

A right parallelepiped enclosure (Fig. 2) with dimensions $l_x=0.976$ m, $l_y=0.695$ m, and $l_z=1.188$ m was used in both numerical simulations and experiments. The enclosure was composed of six plywood boards, 2 in. thick each. Five of them were bolted together to form a cavity and one of them was made removable as a cover. To prevent any possible leakage, sound-proof strips were used in the connecting surfaces between the bolted boards and the removable board, and silicon gel was also used at the connection corners of bolted boards. A square hole of 100×100 mm^2 was cut at (100,59) mm in the cover through which a loudspeaker was installed to create a primary sound field in the enclosure. The Q-factors of the enclosure modes were obtained from measured frequency response function before installing the resonator (see Table I). For each mode, its Q-factor is defined as the resonance frequency divided by the bandwidth between its half-power points. Because of the increasing modal density at higher frequencies, the Q-factors for higher-order modes were assumed to be 45, which is the same as the

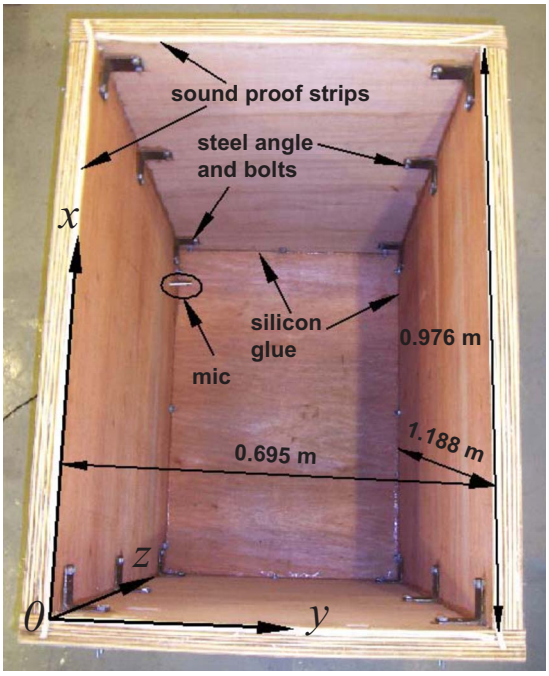

FIG. 2. (Color online) Enclosure used in simulations and experiments.

measured Q-factor for mode (2, 0, 1). Given an ambient temperature of 20 °C and the humidity of 90%, the sound speed was determined as 344.5 m/s. The air density ρ_0 was 1.205 kg/m^3.

The enclosure mode (1, 0, 1) at the predicted natural frequency of 228.4 Hz was chosen as the targeted mode in simulations. A HR having the same frequency of 228.4 Hz was designed. The internal neck diameter of the resonator is 21 mm and the physical neck length is 52 mm. The body of the resonator is a circular tube having a 73.5 mm internal diameter and a 74.1 mm depth. The resonator was installed at (100,300,0) mm.

In simulations, 216 enclosure modes were used, as determined by a convergence study. The eigenfunctions $\varphi_j(\mathbf{r}^R)$ of the enclosure, having thermalviscous boundary conditions, were given in Ref. 14. The calculated natural frequencies of the first 13 modes are tabulated in Table I. The SPL inside the enclosure was evaluated at one arbitrary point (816,70,1028) mm. The predicted baseline SPL at the same location without the resonator is shown in Fig. 3, in which four major peaks correspond to the first four enclosure modes.

TABLE I. Computed natural frequencies and measured Q-factors of the enclosure.

Index	Mode number (lmn)	Natural frequency (Hz)	Q-factor
1	000	0	⋯
2	001	145	32
3	100	176.5	42
4	101	228.4	44
5	010	247.8	46
6	011	287.1	84
7	002	290	42
8	110	304.3	51
9	111	337	79
10	102	339.5	60
11	200	353	80
12	012	381.5	60
13	201	381.6	45
⋯	⋯	>400.0	45

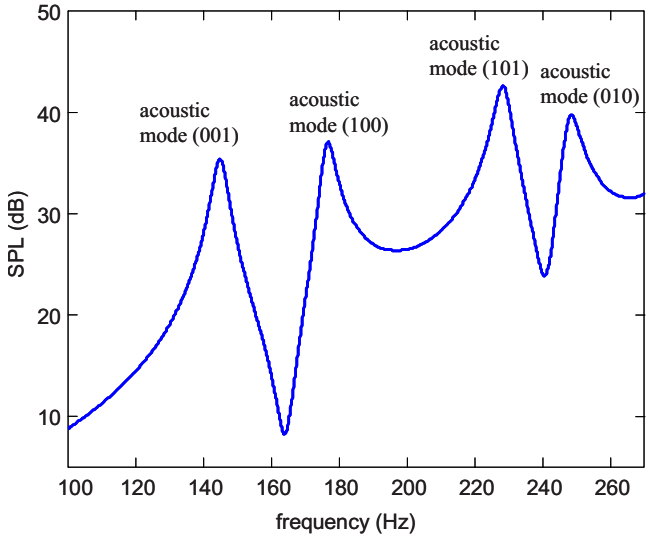

FIG. 3. (Color online) Predicted baseline SPL at (816,70,1028) mm.

A. Experimental validation

The effect of the internal resistance of the resonator is first demonstrated and experimentally validated for a chosen frequency bandwidth of 20 Hz centered at 228.4 Hz. By choosing three typical R_i values (2.25, 3.82, and 9.62 mks Rayls), the SPL variations are shown and compared to the case without resonator in Fig. 4. Note that the case corresponding to R_i=3.82 mks Rayls was obtained as a result of optimization, which will be detailed later in Sec. III B. Figure 4 shows that a 5.8 dB reduction in SPL is achieved when the resonator takes the optimal resistance value of 3.82 mks

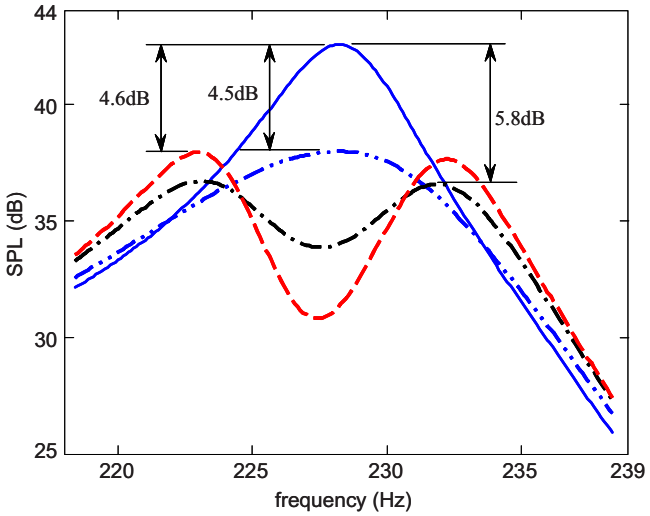

FIG. 4. (Color online) Predicted SPL curves at (0.816,0.07,1.028) m:—without resonator;—·—with a damped resonator, R_i=3.82 mks Rayls; – – with an empty-neck resonator, R_i=2.25 mks Rayls; and —··— with a damped resonator, R_i=9.62 mks Rayls.

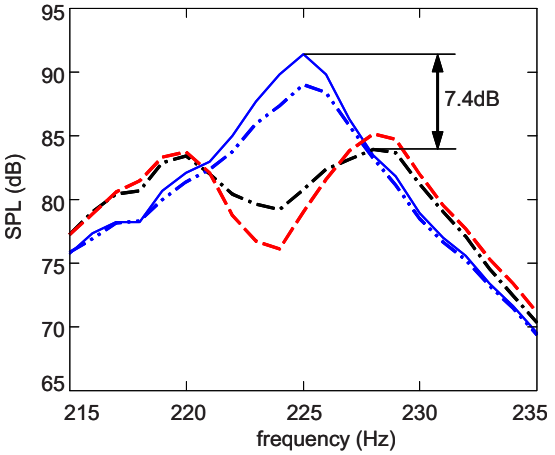

FIG. 5. (Color online) Measured SPL curves at (0.816, 0.07, 1.028) m:—without resonator; —·— with a damped resonator, R_i=3.59 mks Rayls; – – with an empty-neck resonator, R_i=2.25 mks Rayls; and —··— with a damped resonator, R_i=9.62 mks Rayls.

Rayls. When R_i is increased to 9.62 mks Rayls, the performance of the resonator deteriorates, resulting in a 4.5 dB reduction in SPL. With a lightly damped resonator (R_i =2.25 mks Rayls), two sharp peaks appear. This is not acceptable since usually an overall reduction in the frequency band of interest is required.

Experimental measurements were conducted to validate the above predicted results. Similar to the simulation, the enclosure mode (1, 0, 1) was chosen as the targeted mode at the measured natural frequency of 225 Hz. Three resonators, all having a resonance frequency of 225 Hz but different internal resistances, were designed, fabricated, tuned, and installed at (100, 300, 0) mm, respectively. Thin layers of damping material (loudspeaker grill) were inserted in the resonator's neck to produce different internal resistances. For each case, the Q-factor of the resonator was first determined from its measured frequency response curves, which were then used to compute the internal resistance of the resonator.[11] Since it was difficult to fabricate a resonator having exactly the same optimal internal-resistance value as that used in the simulation, the optimal configuration being tested slightly differs from the one used in the simulation. The first resonator has an empty neck, with R_i=2.25 mks Rayls, lower than the theoretically determined optimal value R_{opt} =3.82 mks Rayls. For the second resonator, R_i=3.59 mks Rayls, close to R_{opt}. The third resonator has a R_i=9.62 mks Rayls, which is higher than R_{opt}.

A Brüel & Kjær type 4189 $\frac{1}{2}$ in. microphone was installed at (816, 70, 1028) mm to collect the SPL inside the enclosure. Figure 5 shows the measured SPL curves. Similar to prediction, the resonator with R_i close to the optimal resistance outperforms the other two resonators, resulting in a 7.4 dB reduction in SPL. The other two resonators with either lower or higher R_i than R_{opt} produce changes in the SPL in a very similar manner as numerically predicted. Comparing the predicted SPL curves shown in Fig. 4 with the measured results shown in Fig. 5, the same tendency is found. When the resistance of the resonator is the optimal value or approximates the optimal value, the noise reduction is maximum and the peaks at the coupled frequencies are relatively flat, such resulting in an overall sound reduction within the frequency band. When the internal resistance of the resonator is much lower than the optimal value, the insertion of the resonator produces two pronounced peaks, such affecting the sound attenuation ability of the resonator within the chosen band. In this case, most of energy is radiated back to the enclosure with little amount of energy dissipated by the resonator. Excessive R_i also jeopardizes the effect of the resonator. This attributes to the low mobility of the resonator aperture so that the resonator and the enclosure cannot be effectively coupled. Generally speaking, numerical predictions agree well with measured data. Therefore, the model shows its reliability to guide the resonator design.

B. Analyses

1. Effect of the internal resistance on ER

A 20 Hz bandwidth centered at 228.4 Hz is first chosen as the frequency band of interest for optimization. The internal resistance of the resonator was varied from 0.55 to 50 mks Rayls in the simulation. With the variation in the resonator resistance, the ER was calculated by Eq. (19) and the radiated energy and dissipated energy were also calculated using Eqs. (5a)–(5c) and (13) based on the measured Q-factors of the enclosure, respectively. Notice that the acoustic energy w was computed using Eq. (7). Figures 6(a)–6(c) show the ER inside the enclosure, band-averaged dissipated energy by the resonator, and band-averaged energy radiated from the resonator versus the internal resistance R_i respectively. A maximum reduction of 3.0 dB in ER is observed from Fig. 6(a) when R_i=3.82 mks Rayls, which can be referred to as the optimal value. A similar variation trend as that in Fig. 6(a) is observed in Fig. 6(b), except that the maximum energy dissipation occurs at R_i=3.99 mks Rayls, which is 4% higher than the optimal value determined in Fig. 6(a). This confirms that the effect of the resonator on the ER in the enclosure is mainly dominated by the dissipation ability of the resonator for the frequency band considered here. Figures 6(b) and 6(c) also show that a strong coupling between the resonator and the enclosure takes place with lower R_i value, as evidenced by the efficient sound radiation from the resonator aperture. It means that more energy is returned back to the enclosure from the resonator aperture. As R_i increases, however, more energy was dissipated by the resonator and the radiated energy drastically decreases. Excessive R_i significantly reduces the vibration of the aperture and consequently energy transmission to the resonator so that both energy dissipation inside the resonator and energy radiation from resonator are compromised.

2. Effect of bandwidth

The 20 Hz bandwidth which was previously used covers both the original resonance peak and the newly emerged peaks due to the insertion of the resonator. Should a narrower frequency band be used, it was observed that it has significant impact on the physical effect of the HR as well as the optimal values of its internal resistance. This issue is systematically investigated in this section.

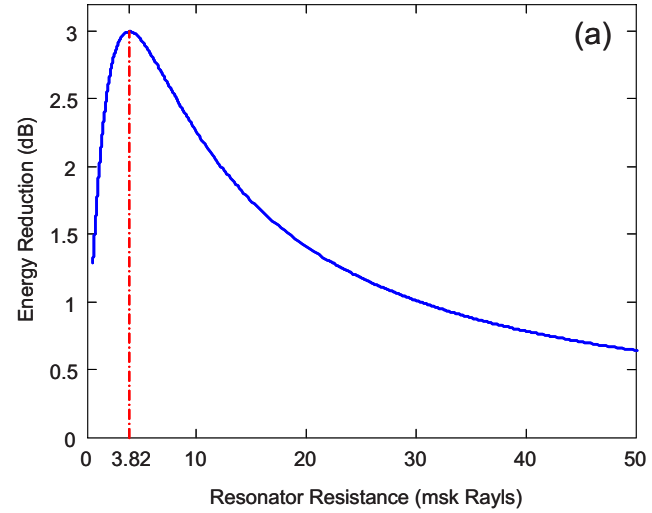

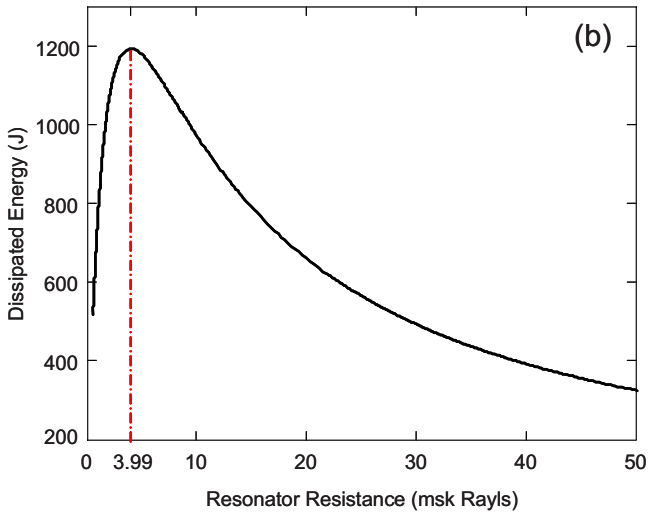

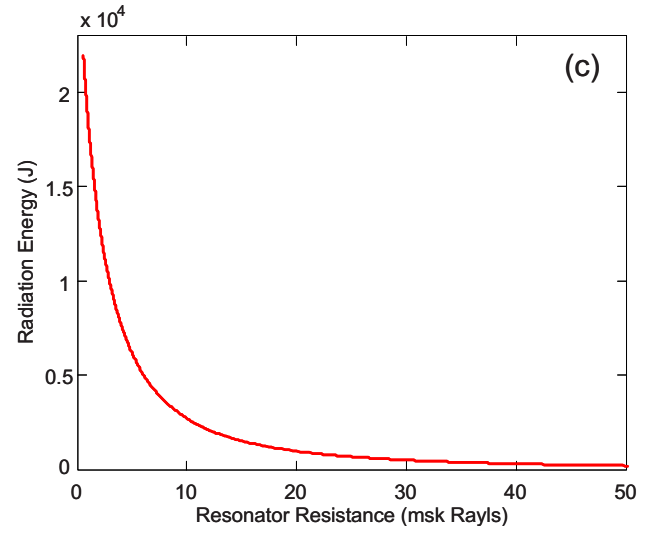

FIG. 6. (Color online) Energy computed in the frequency band of 20 Hz: (a) ER in the enclosure, (b) dissipated energy by the resonator, and (c) radiated energy from the resonator.

The frequency bandwidth was varied from 0.2 to 30 Hz and centered at the targeted resonance of 228.4 Hz. For each frequency band, the internal resistance of the resonator was obtained in two different ways. First, it was determined by

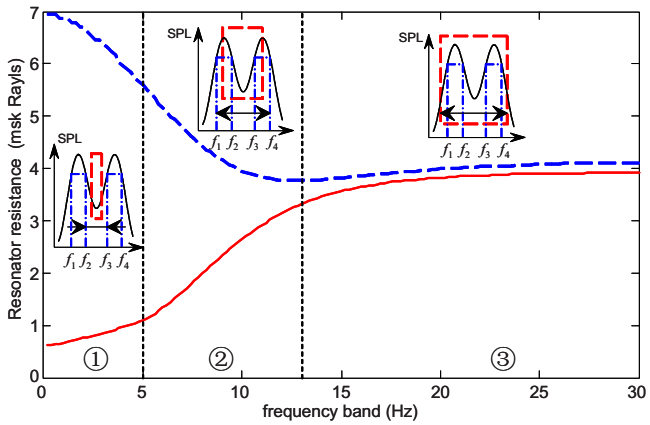

FIG. 7. (Color online) Effect of the chosen frequency band on the resonator resistance: — optimal internal resistance from maximum ER and – – the internal resistance having maximum energy dissipation.

maximizing ER within each frequency band, resulting in the so-called optimal resistance R_{opt}. Second, it was determined by maximizing the energy dissipation by the resonator, giving a resistance value denoted by R_{dis}. R_{opt} and R_{dis} are compared in Fig. 7 with respect to the bandwidth. In order to better quantify the effect of the bandwidth on R_{opt}, Fig. 7 is divided into three different zones, with reference to the half-power frequency bandwidths (denoted by f_2-f_1 and f_4-f_3 in the figure) of the two newly emerged peaks. Zone 3 is featured by a relatively large frequency band completely covering the two new peaks, such as the 20 Hz case which was investigated previously. Within this zone, R_{opt} undergoes slight changes and is relatively close to R_{dis}. This observation is consistent with the analyses carried out in Sec. III B 1, which suggests a dominance of the energy dissipation effect of the resonator. It should be cautioned, however, that even in this case, an accurate determination of R_{opt} cannot be simplified as a problem of maximizing energy dissipation of the resonator, as demonstrated previously in Fig. 6. As opposed to zone 3, zone 1 corresponds to a very narrow band, which only covers the original resonance peak and its very close vicinity. It can be seen that R_{opt} is relatively low, corresponding to lightly damped resonator, and differs significantly from R_{dis}. The low R_{opt} and the apparent difference with R_{dis} indicate that the dissipation of the resonator becomes weak, while the radiation of the resonator becomes strong, resulting in a strong interaction between the resonator and the enclosure. In this case, the targeted resonance peak is sharply split into two new and closely spaced peaks, as illustrated previously in Fig. 4. Meanwhile, the response level inside the enclosure at the targeted resonance is significantly reduced at the expense of creating two high level peaks. Zone 2, which confines the frequency region between the two coupled peaks generated by the insertion of the resonator, is a transition region from narrow band to broad band. Within this zone, R_{opt} undergoes drastic changes, rapidly approaching R_{dis} as the frequency bandwidth increases, suggesting the increasing importance of the energy dissipation.

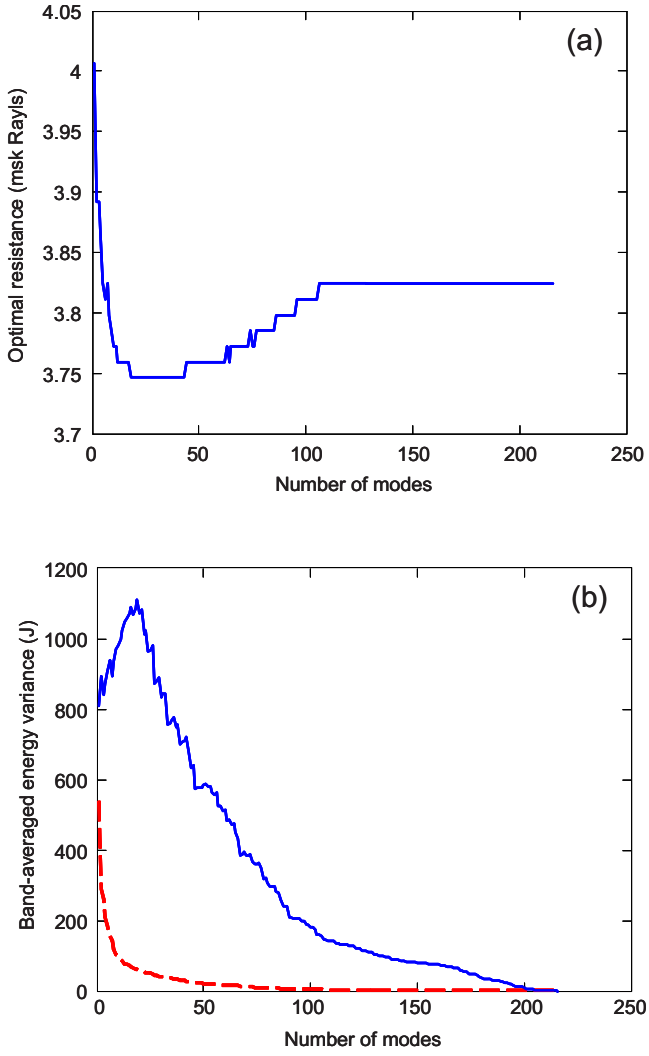

FIG. 8. (Color online) Effect of the modal coupling on (a) optimal resistance of the resonator and (b) band-averaged EV: – – without resonator and — with a resonator, R_i=3.82 mks Rayls.

3. Effect of the modal coupling

As mentioned before, the current model takes into account the multiple modes of the enclosure for HR design. To show this necessity, the effect of modal coupling is investigated.

Figure 8(a) shows the variation in the R_{opt} for 20 Hz bandwidth centered at 228.4 Hz, with the number of the enclosure modes used in the calculation. Enclosure modes used for the sound pressure decomposition are determined according to their closeness to the targeted central frequency to truncate the decomposition series. It can be seen that R_{opt} converges only when a sufficient number of enclosure modes are considered. This suggests that reliable R_{opt} cannot be obtained by only considering the targeted mode or a very limited number of enclosure modes. This phenomenon is apparently due to the choice of a frequency band as performance optimization target instead of one particular frequency, which inevitably enhances the effect of more distant modes. Another plausible explanation may lie in the fact that modal coupling is enhanced due to the insertion of the resonator. This surmise can be ascertained by examining the acoustic energy variation (EV) within the enclosure before and after the resonator is deployed. To this end, a band-averaged EV term is defined as

$$\text{EV} = \frac{1}{\omega_2 - \omega_1}\int_{\omega_1}^{\omega_2} |w - w_0| d\omega, \tag{20}$$

where w and w_0 are the acoustic energies inside the enclosure when a certain number of enclosure modes and 216 enclosure modes are used, respectively. The EV reflects the deviation of the predicted pressure field to the converged state both in frequency and the spatial domains because of the integration in the frequency band and the enclosure volume. The EV was calculated before and after the resonator was used, with comparison given in Fig. 8(b) with respect to the number of enclosure modes. It is seen that when the resonator is absent, the EV inside the enclosure converges rapidly, suggesting that only a small number of enclosure modes actively contribute to system response. Upon insertion of the resonator, however, more modes are activated. This indicates that the insertion of the resonator enhances the modal coupling strength among the enclosure modes through effective interactions with the resonator, as reflected by the second item of Eq. (2).

It is therefore concluded that the consideration of multimodal coupling is necessary in the resonator design when a band performance is expected. One can surmise that this coupling effect will be less apparent if the frequency band of interest becomes narrower.

C. Comparison with Fahy and Schofield's model

It is relevant to compare the present model proposed in this paper and the ones suggested by Fahy and Schofield.[11] Under the assumption of modal separation, Fahy and Schofield proposed two methods to determine the internal resistance of the resonator. (A) For resonance control, the dissipated power at the targeted resonance frequency by the resonator was maximized, leading to

$$Q^R Q^E \varepsilon^2 = 1 \tag{21}$$

and a design chart to choose Q^R. (B) For band control, modal responses at the new coupled frequencies and the original resonance frequency were equalized, leading to an equation

$$\varepsilon Q^E = \frac{2(\varepsilon Q^R)^3}{1 - (\varepsilon Q^R)^2 - (\varepsilon Q^R)^4}. \tag{22}$$

The present work differs from Fahy and Schofield's ones mainly in two aspects: one is the consideration of multiple modal coupling and the other one is the use of a different optimization objective function. It is therefore important to assess and compare the band-control ability of these models.

To this end, the optimal internal resistances of resonators were determined using the current model and Fahy and Schofield's methods, respectively. The ER levels were then computed and compared for four resonant frequencies of the enclosure. Each enclosure mode was targeted by one resonator. By varying the neck length, the body volume of the resonator was kept constant of 0.0009 m^3. Parameters used in the calculation are listed in Table II. R_i values determined

TABLE II. Frequency bands and resonator parameters for the first four nonzero modes of the enclosure.

Natural frequency (Hz)	Frequency band (Hz)		Resonator parameters					
	Lower limit	Upper limit	Diameter of neck (mm)	Diameter of body (mm)	Body volume (m^3)	Location (m)		
						x	y	z
145	135	155	36	100	0.0009	0.964	0.013	1.188
176.5	166.5	186.5				0	0.013	0.1
224.8	214.8	234.8				0.1	0.3	0
247.8	237.8	257.8				0.1	0	0.1

by above three models and the corresponding ER values are listed in Table III. Figure 9 shows the ER levels at each targeted mode. It can be seen that the present model leads to the best sound reduction performance among three cases.

The SPL curves corresponding to the frequency band around 228.4 Hz were chosen for deeper analyses in Fig. 10. It can be seen that Fahy and Schofield's resonance-control method maximizes the dissipated power at the targeted frequency and results in a large resistance and a 5.9 dB peak reduction in SPL. On the contrary, Fahy and Schofield's band-control approach results in a low resistance and consequently produces two pronounced peaks with similar amplitudes. The optimal resistance from the current model provides a 7.9 dB reduction in the frequency band of interest, and a broad band behavior is also observed.

It is also observed that the resistances predicted by Fahy and Schofield's resonance-control model and band-control model give, respectively, the upper and lower bounds for the optimal resistance. In the former case, the resistance is independent of the resonator volume since $Q^R Q^E \varepsilon^2 = 1$, $\varepsilon^2 = \varphi_j^2(\mathbf{r}^R) V^R / \Lambda_j V^E$ and $R_i = \rho_0 c^2 Q^E S^R \varphi_j^2(\mathbf{r}^R) / \Lambda_j V^E \omega^R$. Other models, including the present one, are volume dependent. Figure 11 shows the variation in the optimal resistances, determined using the current model and Fahy and Schofield's models, versus the body volume of the resonator for the targeted enclosure mode (1, 0, 1) at 228.4 Hz. The optimal resistance generally decreases when the volume of the resonator increases, as suggested by the present model. Fahy and Schofield's resonance-control model seems to better apply to the cases where very small resonators are used. With large resonators, Fahy and Schofield's band-control model seems to better approach the true optimal resistance value.

IV. CONCLUSIONS

Based on the analytical solution of a resonator-enclosure interaction model, the effects of internal resistance of a HR on acoustic ER within an enclosure and on the resonator design are investigated. Main conclusions are summarized as follows:

(1) The model and design methodology proposed in this paper allow maximization of the acoustic ER inside an enclosure within a frequency band around a resonance frequency. It provides a good cutoff between the peak reduction and the resonator working bandwidth. Numerical predictions are in fair agreement with experiments.
(2) When the frequency band of interest is wide enough (zone 3), which covers both the original resonance peak and the newly emerged peaks caused by the insertion of the resonator, the dissipation ability of the resonator dominates its control performance, which greatly depends on both the internal resistance of the resonator neck and the vibrating velocity of the lumped mass in the neck. While acknowledging the importance of energy dissipation, the determination of the optimal internal resistance of the resonator cannot simply be trimmed down to the maximization of energy dissipation. A narrow band of interest (zone 1), however, requires a lightly damped resonator, which promotes more energetic interaction with the enclosure.
(3) The insertion of the resonator in an acoustic enclosure enhances the modal coupling strength among the acoustic modes of the cavity. It is therefore necessary to consider a sufficient number of acoustic modes to achieve an

TABLE III. Optimal R_i and ER of three different models for the first four nonzero modes of the enclosure.

Natural frequency (Hz)	Current model		Fahy and Schofield's model			
			Resonance control		Band control	
	Optimal R_i (mks Rayls)	ER (dB)	Optimal R_i (mks Rayls)	ER (dB)	Optimal R_i (mks Rayls)	ER (dB)
145	10	2	12.7	2	1.25	0.9
176.5	6.4	3.9	13.7	3.2	0.95	1.3
224.8	5.93	5.4	19.94	3.4	1.1	2.9
247.8	3.52	5.5	11.39	3.7	0.65	3.6

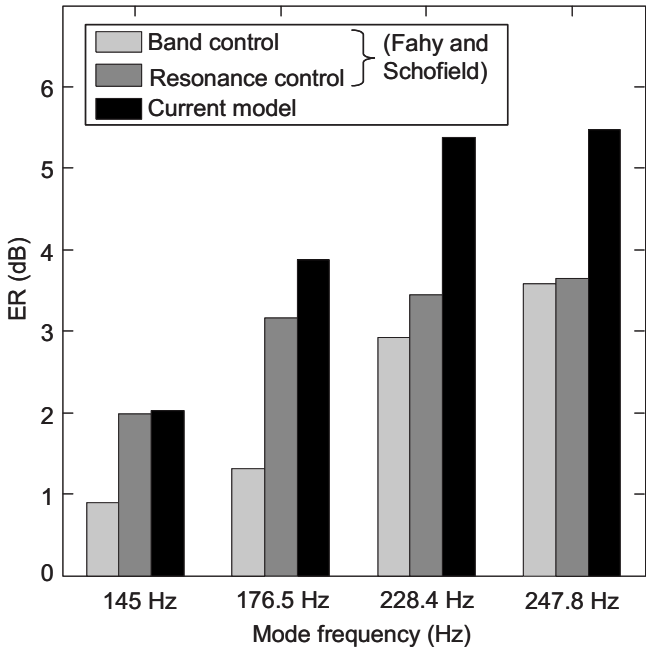

FIG. 9. Comparison of different models in terms of ER.

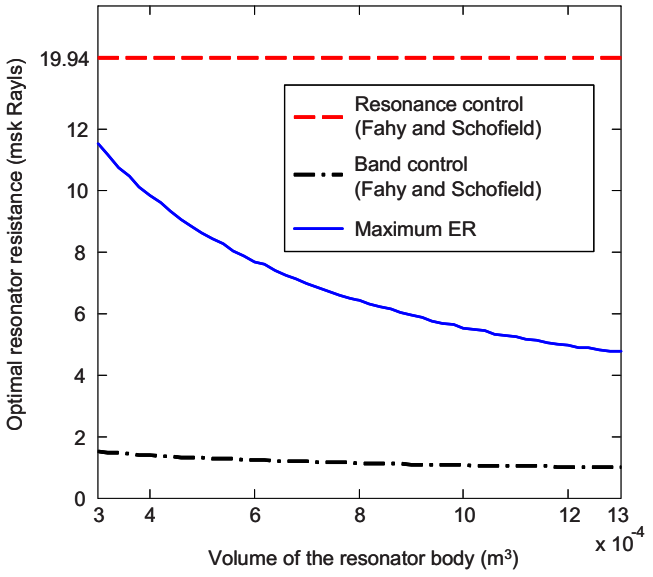

FIG. 11. (Color online) Variation in optimal resonator resistance with respect to the body volume of the resonator for the targeted enclosure mode (1, 0, 1) at 228.4 Hz.

optimal design of the resonator. This becomes increasingly important when the frequency band of interest is large.

(4) Compared with the model proposed in this paper, the two models provided by Fahy and Schofield are found to provide the upper and lower bounds of the optimal resistance. The applicability of the two models depends on the volume of the resonators.

ACKNOWLEDGMENTS

The authors wish to acknowledge a grant from Research Grants Council of Hong Kong Special Administrative Region, China (Project No.PolyU 5137/06E) and support by the Central Research Grant of The Hong Kong Polytechnic University through Grant No.G-YG19.

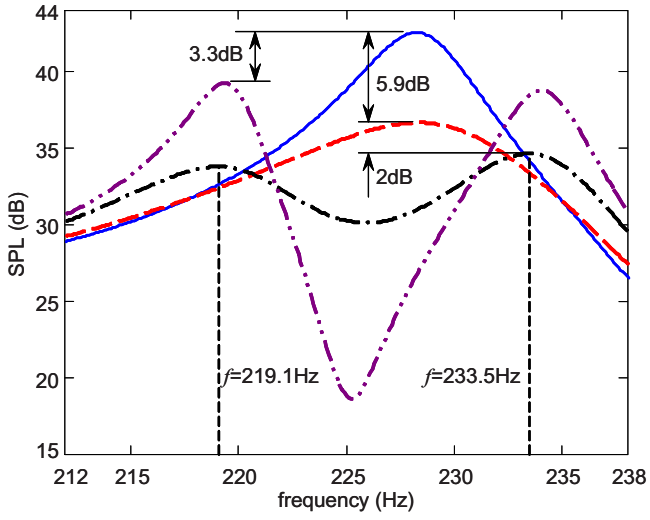

FIG. 10. (Color online) Predicted SPLs at (0.816, 0.07, 1.028) m: — without resonator; – – with resonator, R_i=19.94 mks Rayls from Fahy and Schofield's resonance-control model; —··— with resonator, R_i=1.1 mks Rayls from Fahy and Schofield' band-control model; and —·— with resonator, R_i=5.93 mks Rayls from current model.

[1]S. J. Estève and M. E. Johnson, "Reduction of sound transmission into a circular cylindrical shell using distributed vibration absorbers and Helmholtz resonators," J. Acoust. Soc. Am. **112**, 2840–2848 (2002).
[2]S. H. Seo and Y. H. Kim, "Silencer design by using array resonators for low-frequency band noise reduction," J. Acoust. Soc. Am. **118**, 2332–2338 (2005).
[3]S. R. Kim, Y. H. Kim, and J. H. Jang, "A theoretical model to predict the low-frequency sound absorption of a Helmholtz resonator array (L)," J. Acoust. Soc. Am. **119**, 1933–1936 (2006).
[4]N. Sugimoto, M. Masuda, and T. Hashiguchi, "Frequency response of nonlinear oscillations of air column in a tube with an array of Helmholtz resonators," J. Acoust. Soc. Am. **114**, 1772–1784 (2003).
[5]T. Starecki, "Loss-improved electroacoustical modeling of small Helmholtz resonators," J. Acoust. Soc. Am. **122**, 2118–2123 (2007).
[6]F. Liu, A. Phipps, S. Horowitz, K. Ngo, L. Cattafesta, T. Nishida, and M. Sheplak, "Acoustic energy harvesting using an electromechanical Helmholtz resonator," J. Acoust. Soc. Am. **123**, 1983–1990 (2008).
[7]A. Selamet and I. Lee, "Helmholtz resonator with extended neck," J. Acoust. Soc. Am. **113**, 1975–1985 (2003).
[8]A. Selamet, M. B. Xu, I. J. Lee, and N. T. Huff, "Helmholtz resonator lined with absorbing material," J. Acoust. Soc. Am. **117**, 725–733 (2005).
[9]F. Liu, S. Horowitz, T. Nishida, L. Cattafesta, and M. Sheplak, "A multiple degree of freedom electromechanical Helmholtz resonator," J. Acoust. Soc. Am. **122**, 291–301 (2007).
[10]F. J. Van Leeuwen, "The damping of eigen-tones in small rooms by Helmholtz resonators," European Broadcasting Union Review, A-Technical **62**, 155–161 (1960).
[11]F. J. Fahy and C. Schofield, "A note on the interaction between a Helmholtz resonator and an acoustic mode of an enclosure," J. Sound Vib. **72**, 365–378 (1980).
[12]W. V. Slaton and J. C. H. Zeegers, "Acoustic power measurements of a damped aeroacoustically driven resonator," J. Acoust. Soc. Am. **118**, 83–91 (2005).
[13]S. Griffin, S. A. Lane, and S. Huybrechts, "Coupled Helmholtz resonators for acoustic attenuation," J. Vibr. Acoust. **123**, 11–17 (2001).
[14]A. Cummings, "The effects of a resonator array on the sound field in a cavity," J. Sound Vib. **154**, 25–44 (1992).
[15]D. Li and L. Cheng, "Acoustically coupled model of an enclosure and a Helmholtz resonator array," J. Sound Vib. **305**, 272–288 (2007).
[16]A. D. Pierce, *Acoustics: An Introduction to Its Physical Principles and Applications* (Acoustical Society of America, New York, 1989).